Reproduction of the vibroacoustic response of panels under stochastic excitations using the source scanning technique

A. Pouye, Laurent Maxit, Cédric Maury, Marc Pachebat

▶ **To cite this version:**

A. Pouye, Laurent Maxit, Cédric Maury, Marc Pachebat. Reproduction of the vibroacoustic response of panels under stochastic excitations using the source scanning technique. Journal of Sound and Vibration, 2021, 510, pp.116307. 10.1016/j.jsv.2021.116307 . hal-03290508

HAL Id: hal-03290508
https://hal.science/hal-03290508

Submitted on 21 Nov 2021

HAL is a multi-disciplinary open access archive for the deposit and dissemination of scientific research documents, whether they are published or not. The documents may come from teaching and research institutions in France or abroad, or from public or private research centers.

L'archive ouverte pluridisciplinaire **HAL**, est destinée au dépôt et à la diffusion de documents scientifiques de niveau recherche, publiés ou non, émanant des établissements d'enseignement et de recherche français ou étrangers, des laboratoires publics ou privés.

Distributed under a Creative Commons Attribution - NonCommercial - NoDerivatives 4.0 International License

Reproduction of the Vibroacoustic Response of Panels under Stochastic Excitations using the Source Scanning Technique

Augustin Pouye[a,b,*], Laurent Maxit[a], Cédric Maury[b], Marc Pachebat[b]

[a] *Univ Lyon, INSA–Lyon, Laboratoire Vibrations-Acoustique (LVA), 25 bis, av. Jean Capelle, F-69621, Villeurbanne Cedex, France.*
[b] *Aix Marseille Univ, CNRS, Centrale Marseille, Laboratoire de Mécanique et d'Acoustique (LMA), 38 rue Frédéric Joliot Curie, 13013 Marseille, France.*

Abstract

The reproduction of the vibration and acoustic responses of structures under random excitation such as the diffuse acoustic field or the turbulent boundary layer is of particular interest to researchers and the transportation industry (automobile, aeronautics, etc.). In practice, the characterization of structures under random excitations requires making *in-situ* measurements or using test facilities such as the wind tunnel, which are complex and costly methods. Based on the previous considerations, the necessity of finding a simple, cost-efficient and reproducible alternative methods becomes obvious. The source scanning technique based on a single acoustic source and the synthetic array principle is one of these alternative techniques. The present paper proposes to assess its validity by comparing its results with numerical and experimental ones. An academic case study consisting of a baffled and simply supported aluminum panel under diffuse acoustic field and turbulent boundary layer excitations is considered. The experimental vibration response of the panel as well as the transmission loss using the proposed process are compared to results from random vibration theory on one hand. On the other hand, the same experimental

*Corresponding author.
Email addresses: augustin.pouye@insa-lyon.fr (Augustin Pouye), laurent.maxit@insa-lyon.fr (Laurent Maxit), cedric.maury@centrale-marseille.fr (Cédric Maury), pachebat@lma.cnrs-mrs.fr (Marc Pachebat)

results obtained using the source scanning technique are compared with results obtained with measurements using a reverberant room (diffuse acoustic field) and an anechoic wind tunnel (turbulent boundary layer). These comparisons show good agreement that validate the source scanning technique for the considered panel.

Keywords: Turbulent Boundary Layer, Diffuse Acoustic Field, Vibration Response, Radiated Power, Sound Field Synthesis, Source Scanning Technique

1. Introduction

The experimental characterization of structures under random excitations such as the diffuse acoustic field (DAF) and the turbulent boundary layer (TBL) is of great interest to the transportation industry and the building sector. However, the test facilities generally used (i.e. reverberant chamber for the DAF and wind tunnel or *in-situ* tests for the TBL) can be hard to control and costly. Moreover, the results obtained for a given structure can be very different from one facility to another even though the same setup is implemented.

The reproduction of the vibroacoustic response of structures under stochastic excitations using an array of acoustic sources was theoretically shown some decades ago [1]. But due to technical limitations, this method could not be experimentally validated. Since 2000, several researchers have addressed this problem using various approaches. Maury, Bravo, Elliott and Gardonio [2–5] have widely discussed the reproduction of random excitations using an array of loudspeakers. This method works well when it comes to the reproduction of a DAF excitation but due to the limited number of sources in the array, it fails to simulate the wall-pressure fluctuations of a subsonic TBL excitation because of the high wavenumbers involved meaning that a denser source array would be required. A criteria of approximately four sources per smallest wavelength was derived in the literature in order to reproduce the small correlation lengths of the surface pressure field induced by the TBL [5, 6]. As frequency increases, the number of required sources becomes very large and as one is limited by

the size of the sources, the frequency range that can be studied with a given source is also limited. In order to circumvent this issue, Maury and Bravo [7] proposed a focused synthesis of the TBL excitation over a subdomain of the simulation surface. While this method allows to reach higher frequencies and ensures correct reproduction of the TBL excitation, it also limits the observation area to a fraction of the actual panel. Other methods using arrays of acoustic sources have been proposed over the years [8–10]: the *wave field synthesis* (WFS) and the *planar nearfield acoustic holography* (P-NAH) which are both open-loop processes. They provide good reproduction results in the case of the DAF but they are still not able to accurately synthesize the wall-pressure field induced by a TBL excitation outside the acoustic wavenumber domain.

On another hand, Marchetto et al. [11, 12] developed an alternative approach aiming at experimentally predicting the vibration response of panels under DAF and TBL excitations by separating the contributions of the wall-pressure excitation from the vibration behavior of the panel through a mathematical formulation in the wavenumber domain. In this formulation the excitation is characterized by its cross-spectral density function whereas the vibratory behavior of the panel is given by its sensitivity functions which are experimentally measured indirectly using variations of the reciprocity principle: here, the sensitivity functions were determined by exciting the structure at the point of interest and measuring the response with a laser vibrometer on a grid of points on the structure [13]. The results obtained with this approach were compared to results from test facilities and there was a fairly good agreement between both kinds of results and for both types of excitations. However, the approach remains experimentally time consuming as the vibratory field of the panel for each position of the excitation has to be measured in order to determine the transmission loss of the considered structure.

Aucejo et al. [6] had a different approach from the previous ones. Instead of using a compact source array with a predefined number of sources, only one monopole source was used along with the synthetic array principle [14]. This process that requires two identification steps uses the concept of synthetic array

to simulate TBL-induced vibrations from a set of transfer functions. It was named the source scanning technique (SST) and was applied to reproduce the vibration response of a steel panel to a TBL excitation in the low frequency domain (up to 300 Hz). This approach differs from the one presented in [12] by the fact that the sensitivity functions are measured directly, that is to say without using reciprocity principles of [12]. The reproduction of wall-pressure plane waves and a qualitative comparison of the response at a given point on the panel subject to a TBL excitation with measurements taken from the literature were done. The experimental conditions, particularly the boundary conditions were not very well mastered, hence only qualitative comparisons could be carried out in [6]. While these first results were promising, SST requires yet evidence of validation in order to be adopted as an alternative mean to the standard ones. The present paper proposes to fill this gap. An extensive study of SST is achieved on a wider frequency range. In order to validate this experimental approach, the results obtained with SST are compared to numerical results and experimental ones (obtained from measurements in reverberant room and anechoic wind tunnel). In a first step, a parametric study based on numerical simulation allows us to define the optimal number of sources as well as the optimal position of the array from the panel. In a second step, the results of the proposed experimental process are compared to numerical simulations of the vibration response of the panel as well as its radiated power. In a last step, the vibration results are compared with measurements in a reverberant room for the DAF case and in a wind tunnel for the TBL case.

This paper is organized as follows: first the theoretical background on the vibroacoustic response of a panel under random excitation is given. Secondly, the source scanning technique is briefly described along with some parametric studies aiming at facilitating the choice of the ideal setup for the reproduction of the vibroacoustic response of a panel under a given excitation. Finally, after presenting the experimental setup, the vibroacoustic response as well as the radiated power determined using the proposed approach are compared to numerical results as well as experimental results obtained from test facilities

(reverberant chamber and wind tunnel).

2. Wavenumber formulation and definition of the quantities of interest

This analysis considers the response of two dimensional rectangular structures to a random pressure field excitation. This pressure field is assumed to be stationary in time and homogeneous in space. We will be interested in two types of random excitations: the diffuse acoustic field and the turbulent boundary layer excitation. The quantities of interest will be the auto-spectral density (ASD) function of the velocity at one point on the panel and the radiated sound power.

The geometric configuration of the studied structure of surface Σ_p is shown in Fig. 1. In the following, we will assume that the wall-pressure fluctuations are not affected by the vibrations of the structure which means that the excitation is not modified by the structural response. Thus the random excitations considered in this paper are modeled by the wall pressure fluctuations that would be observed on a smooth rigid wall, also known as the *blocked pressure* p_b [15].

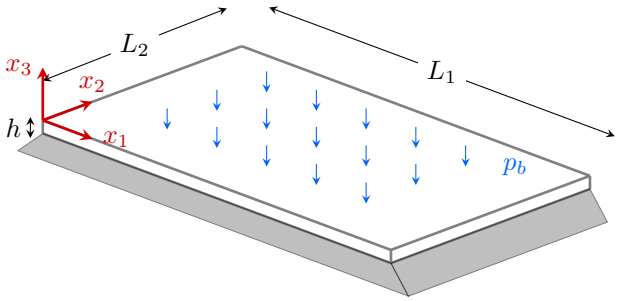

Figure 1: Simply supported panel subject to an excitation p_b.

2.1. Response of panels to random pressure fields

Considering the hypotheses stated above and the random vibration theory, the space-frequency spectrum of the panel response, $S_{\alpha\alpha'}(\mathbf{x}, \omega)$ can be written

[16, 17]

$$S_{\alpha\alpha'}(\mathbf{x},\omega) = \frac{1}{4\pi^2}\iint_{-\infty}^{+\infty} H_\alpha(\mathbf{x},\mathbf{k},\omega)\, S_{p_b p_b}(\mathbf{k},\omega)\, H^*_{\alpha'}(\mathbf{x},\mathbf{k},\omega)\,\mathrm{d}\mathbf{k} \tag{1}$$

where α and α' denote either, v, the panel velocity, p, the radiated pressure or v_0, the acoustic velocity in the x_3 direction and

$$H_\alpha(\mathbf{x},\mathbf{k},\omega) = \iint_{\Sigma_p} \Gamma_\alpha(\mathbf{x},\mathbf{y},\omega)\, e^{-j\mathbf{k}\mathbf{y}}\mathrm{d}\mathbf{y} \tag{2}$$

is called sensitivity function and characterizes the vibroacoustic behavior of the panel. From Eq. (2), one can deduce that it corresponds to the response α of the considered system at point $\mathbf{x}$ when it is excited by a unit wall plane wave of wavevector $\mathbf{k}$ at the angular frequency ω. The integral in Eq. (1) can approximated by the rectangular rule. The space-frequency spectrum of the panel response can then be estimated by

$$S_{\alpha\alpha'}(\mathbf{x},\omega) \approx \frac{1}{4\pi^2}\sum_{\mathbf{k}\in\Omega_\mathbf{k}} H_\alpha(\mathbf{x},\mathbf{k},\omega)\, S_{p_b p_b}(\mathbf{k},\omega)\, H^*_{\alpha'}(\mathbf{x},\mathbf{k},\omega)\,\delta\mathbf{k} \tag{3}$$

where $\Omega_\mathbf{k}$ is a set of properly chosen wave-vectors.

This expression will allow us to estimate the panel response under the stochastic excitation from the knowledge of the sensitivity functions $H_\alpha(\mathbf{x},\mathbf{k},\omega)$ and the wavenumber-frequency spectrum of the wall-pressure field $S_{p_b p_b}(\mathbf{k},\omega)$. It can be emphasized that other numerical methods as the trapezoidal and Simpson's rules can be used to approximate the integral of Eq. (1). However, for the cases considered in the present study, and for the wavenumber resolution, δ_k defined in Sec. 3.2.1, they give very similar results to the ones obtained using the rectangular rule. In the next two subsections, one describes $S_{p_b p_b}(\mathbf{k},\omega)$ for the DAF and the TBL whereas one will describe in Sec. 3 how to determine the sensitivity functions with the source scanning technique.

2.1.1. Diffuse acoustic field

This excitation is commonly used to determine the sound reduction index of panels as described in several standards using coupled reverberant-reverberant room [18, 19] or reverberant-anechoic room [20, 21] laboratory facilities. The

DAF excitation is also encountered in transportation vehicles such as aircraft, satellite, high speed trains, and cars. Theoretically, it is defined as an infinite set of uncorrelated acoustic plane waves with equipropable incident angles. There is a closed-form solution that exactly describes it. The frequency-wavenumber spectrum of the DAF blocked-pressure [22, 23] is written

$$S_{p_b p_b}(\mathbf{k},\omega) = \begin{cases} \dfrac{2\pi}{k_0} \dfrac{\Phi_{p_b p_b}(\omega)}{\sqrt{k_0^2 - |\mathbf{k}|^2}} & \text{if } |\mathbf{k}| < k_0 \\ 0 & \text{if } |\mathbf{k}| \geq k_0 \end{cases} \tag{4}$$

where $\Phi_{p_b p_b}(\omega)$ is the ASD function of the wall-pressure fluctuations, $k_0 = \omega/c_0$ is the acoustic wavenumber and c_0 the speed of sound in the medium; $|\mathbf{k}| = \sqrt{k_1^2 + k_2^2}$, k_1 and k_2 are the wavenumbers in the x_1 and x_2 directions, respectively. For the numerical applications as well as for the presentation of the experimental results, one will consider a unit wall pressure ASD function (i.e. $\Phi_{p_b p_b}(\omega) = 1\,\mathrm{Pa}^2\,\mathrm{Hz}^{-1}$) in the following.

2.1.2. Turbulent boundary layer

There are numerous TBL models available in the literature. Nevertheless, none of these models can perfectly match the pressure fluctuations due to an experimentally simulated TBL excitation without undergoing some parametric changes. In order to reduce the uncertainties as much as possible, one will use a model of Mellen [24] that was fitted, in a previous study, to measurements in the anechoic wind tunnel of the University of Sherbrooke [12]. The frequency-wavenumber spectrum of the wall-pressure fluctuations is then given by

$$S_{p_b p_b}(\mathbf{k},\omega) = \frac{2\pi (\alpha_1 \alpha_2)^2 k_c^3 \Phi_{p_b p_b}(\omega)}{\left[(\alpha_1 \alpha_2 k_c)^2 + (\alpha_1 k_2)^2 + \alpha_2^2 (k_c - k_1)^2\right]^{3/2}} \tag{5}$$

The parameters of this model, namely the spatial coherence decay rates α_1 and α_2, the convective wavenumber $k_c = \omega/U_c$ where U_c is the convection velocity, and the wall-pressure ASD $\Phi_{p_b p_b}(\omega)$ were fitted to measurements in wind tunnel aiming at characterizing the wall-pressure fluctuations induced by a subsonic turbulent flow excitation with a free stream velocity $U_\infty = 20\,\mathrm{m\,s}^{-1}$.

See Ref. [12] for more details about these measurements and for the values of α_1, α_2 and U_c. These fitted Mellen parameters will be considered in the following applications.

2.2. Radiated power

The radiated power is defined by the following equation

$$\Pi_r(\omega) = \iint_{\Sigma_p} I_{act}(\mathbf{x}, \omega)\, \mathrm{d}\mathbf{x} \tag{6}$$

where $\mathrm{d}\mathbf{x}$ is the surface element and $I_{act}(\mathbf{x}, \omega)$ is the normal component of the active sound intensity at point $\mathbf{x}$. The active sound intensity is directly related to the cross-spectrum density (CSD) function $S_{pv_0}(\mathbf{x}, \omega)$ between the sound pressure and the particle velocity at point $\mathbf{x}$ [25]

$$I_{act}(\mathbf{x}, \omega) = \mathrm{Re}\left[S_{pv_0}(\mathbf{x}, \omega)\right] \tag{7}$$

where $\Re$ designates the real part and from Eq. (3), one has

$$S_{pv_0}(\mathbf{x}, \omega) \approx \frac{1}{4\pi^2} \sum_{\mathbf{k} \in \Omega_\mathbf{k}} H_p(\mathbf{x}, \mathbf{k}, \omega)\, S_{pp}(\mathbf{k}, \omega)\, H^*_{v_0}(\mathbf{x}, \mathbf{k}, \omega)\, \delta\mathbf{k} \tag{8}$$

In practice, the radiated power will be estimated by an approximation of the integral of Eq. (6) with the rectangular rule

$$\Pi_r(\omega) \approx \sum_{\mathbf{x} \in \Sigma_r} I_{act}(\mathbf{x}, \omega)\, \delta\mathbf{x} \tag{9}$$

where Σ_r is an elemental surface at a distance x_3 on the radiating side of the panel.

3. Source Scanning Technique

3.1. Principle

In this section, one describes the process of the source scanning technique that will allow us to measure the panel sensitivity functions that intervene in Eq. (3).

The synthetic array principle consists in using a single monopole source which is spatially displaced to different positions thereby creating virtually the array of monopole sources. It is closely related to the concept of *Synthetic Aperture Radar* (SAR), which consists in post-processing the signals received by a moving radar to produce fine resolution images from an intrinsically resolution-limited radar system in the along-track direction [14, 26].

The proposed approach is based on the mathematical formulation of the problem in the wavenumber domain. This formulation is appropriate because it allows, through Eq. (3), an explicit separation of the contributions of the excitation *via* the wall-pressure CSD function from those of the vibroacoustic behavior of the structure *via* the sensitivity functions discussed above.

Let us consider a unit wall plane wave characterized by the wave-vector, $\mathbf{k}$ and the angular frequency ω. The pressure at the surface of the panel that will be referred to as the reproduction surface, is simply given by: $p(\mathbf{x}, \mathbf{k}, \omega) = e^{-i\mathbf{kx}}$. The SST process is based on four steps that will allow us to reproduce this target pressure field from S position s of the monopole source.

(1) **Definition of the target pressure at the observation points:** one supposes that the reproduction surface is regularly discretized in P observation points and one defines the target pressure vector as the vector with the components corresponding to the pressure of the unit wall plane wave at the P points. The spacing between the points should be sufficiently small to describe the spatial variation of the wall plane wave. Numerical investigations have shown that at least 2 points per wavelength is a minimum requirement.

(2) **Characterization of the acoustic source:** one measures the transfer functions (G_{ps}) between source positions $s \in [1, S]$ and observation points $p \in [1, P]$ on the panel (microphones), see Fig. 2. In this paper, the transfer function, G_{ps} is defined as the ratio of the pressure at point p when the source is located at position s over the input voltage of the source. One defines the transfer function matrix $\mathbf{G}$ as the matrix having the transfer

functions G_{ps} as components.

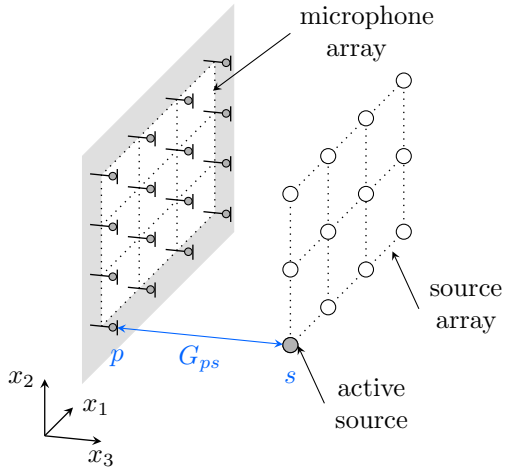

Figure 2: Measurement of $G_{ps}(\omega)$

(3) **Computation of the vector of source amplitudes q** by inverting the following matrix equation

$$\mathbf{Gq} = \mathbf{p} \tag{10}$$

that can be rewritten explicitly

$$\sum_{s=1}^{S} G_{ps}(\omega)\, q_s(\mathbf{k},\omega) = p_p(\mathbf{k},\omega),\ \forall p \in [1,P] \tag{11}$$

where $q_s(\mathbf{k},\omega)$ is the amplitude of the source s and $p_p(\mathbf{k},\omega) = e^{-ik_1 x_1^p - ik_2 x_2^p}$ represents the target pressure at the observation point p which coordinates are x_1^p and x_2^p on the panel.

When the number of observation points P is less than the number of source positions S, the system in Eq. (10) is underdetermined and has an infinite number of solutions. However, when $P > S$, the system is overdetermined and do not have one single exact solution. Nevertheless, a solution minimizing the reproduction error introduced in Sec. 3.2.2 can be determined. The matrix $\mathbf{G}$ is then rectangular, therefore Eq. (10) is solved in the least squares sense as

$$\mathbf{q} = \mathbf{G}^{\dagger}\mathbf{p} \tag{12}$$

The dagger symbol in Eq. (12) indicates the Moore-Penrose pseudo-inverse. The reproduction of a target pressure field using an array of acoustic sources is thus an inverse problem which leads to some issues that will be discussed later on.

(4) **Synthesis of the target pressure field and of the sensitivity function:** in order to assess the quality of the reconstructed pressure field, one considers Q points on the reproduction surface. These Q points can be different from the P reference points in order to estimate the ability of the technique to reproduce correctly the pressure field between the reference points. After the transfer function matrix $\hat{\mathbf{G}}$ between the S source positions and the Q reconstruction points is determined from measurements or numerical simulations, the vector of the reconstructed pressure $\hat{\mathbf{p}}$ can be computed with the following expression: $\hat{\mathbf{p}} = \hat{\mathbf{G}}\mathbf{q}$. One will use this expression in the following to estimate the efficiency of the SST and to define the optimal parameters of the virtual array. However, in practice, it will not be used, as only the sensitivity functions are of interest to estimate the panel response to the stochastic excitation. The sensitivity functions are given by the following equation

$$H_\alpha(\mathbf{x}, \mathbf{k}, \omega) = \sum_{s=1}^{S} q_s(\mathbf{k}, \omega)\, \Gamma_\alpha^s(\mathbf{x}, \omega) \tag{13}$$

where $\alpha = (v, p, v_0)$ and $\Gamma_\alpha^s(\mathbf{x}, \omega)$ represents the frequency response functions (FRFs) between point $\mathbf{x}$ and the source at position s and is defined as the response α at point $\mathbf{x}$ when the source is located at point s over the input voltage of the source.

Step 2 is generally achieved only one time whereas the other steps can be repeated to cover the set of wave-vectors of interest in Eq. (3). Once the sensitivity functions have been estimated by Eq. (13) for the different wave-vectors of interest, the panel response to the stochastic excitation can be estimated with Eq. (3) and the model of the wall-pressure field (as described in the Sec. 2.1.1 and 2.1.2 for the DAF and the TBL, respectively).

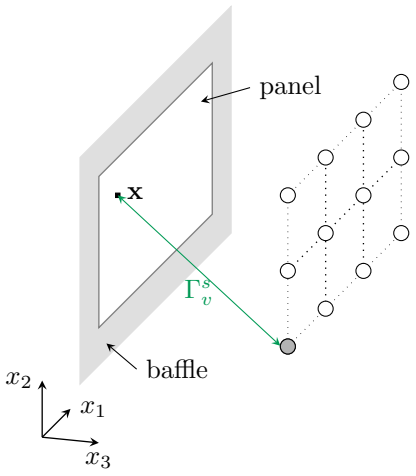

Figure 3: Measurement of the velocity FRF $\Gamma_v^s(\mathbf{x}, \omega)$

3.2. Parametric studies

In the following, some parametric investigations on the SST are proposed. These studies aim at determining the optimal parameters of the array of sources for an accurate reproduction of the vibroacoustic response of the structure. The numerical simulations presented in this section concern a panel with the same geometrical and mechanical properties (see Table 1) as the one we will consider experimentally in Sec. 4. The panel is supposed simply supported on its four edges. The normal modes are then calculated analytically and the sensitivity functions can be estimated using the modal expansion method as described in Appendix A.

3.2.1. Cutoff wavenumber and wavenumber resolution

The minimum separation between the source positions is derived from the maximum wavenumber or the minimum wavelength to be synthesized. For frequencies well above the hydrodynamic coincidence frequency and accordingly to Marchetto et al. [12], the wavenumber domain $\Omega_{\mathbf{k}}$ over which Eq. (3) is calculated must at least include the flexural wavenumber of the panel at the highest frequency of the considered frequency range. The natural flexural wavenumber

Table 1: Panel parameters

Parameter	Symbol	Value
Young modulus	E	68.9 GPa
Poisson ratio	ν	0.3
Mass density	ρ	2740 $\mathrm{kg\,m^{-3}}$
Length	L_1	0.48 m
Width	L_2	0.42 m
Thickness	h	3.17 mm

of a thin panel is given by the following equation

$$k_f(\omega) = \sqrt[4]{\omega^2 \frac{\rho h}{D}} \tag{14}$$

where $D = \dfrac{Eh^3}{12(1-\nu^2)}$ is the flexural rigidity of the panel.

Thus the smallest cutoff wavenumber from which the spacing δ_s between the source positions is defined is set to

$$k_{max} = \beta k_f(\omega_{max}) \tag{15}$$

where β is a safety coefficient such that $\beta > 1$ and ω_{max} corresponds to the maximum frequency of the considered frequency range.

The spacing between two adjacent sources is then defined using the criteria of four monopoles per smallest wavelength (as shown in previous studies [5, 6])

$$\delta_s = \frac{\lambda_{min}}{4} \tag{16}$$

where $\lambda_{min} = 2\pi/k_{max}$.

Let us now talk about the wavenumber resolution. Numerical simulations do not show that the wavenumber resolution is a critical parameter as $H_\alpha(\mathbf{x}, \mathbf{k}, \omega)$ and $S_{p_b p_b}(\mathbf{k}, \omega)$ do not vary quickly with respect to the wavenumber. Moreover, SST can deal with fine resolution as the wavenumber resolution only affects the post-processing steps. In the following, the wavenumber resolution is set to $\delta k_{1,2} = 1\,\mathrm{rad\,m^{-1}}$.

3.2.2. Interplanar distance

The interplanar distance represents the distance between the source array plane and the panel plane (or reproduction plane). The study presented in this section aims at defining the optimal interplanar distance ensuring an accurate pressure synthesis.

In order to assess the quality of the reproduction process, two different parameters are examined:

- The condition number of the transfer matrix $\mathbf{G}$ denoted $\kappa(\mathbf{G})$ which is a measure of the sensitivity of the sought parameters (i.e. the amplitudes of the sources) with respect to perturbations in the input data and round-off errors made while solving Eq. (10) for $\mathbf{q}$. When the condition number is large, the computed solution of the system may be in error. Values of the condition number near one indicate a well-conditioned matrix whereas large values indicate an ill-conditioned matrix [27].

- The relative mean square error (MSE) on the synthesized pressure field denoted e_p is defined by the following equation

$$e_p(k_1, k_2, \omega) = \frac{E\left[\left\|\mathbf{p}(\mathbf{x}, k_1, k_2, \omega) - \hat{\mathbf{p}}(\mathbf{x}, k_1, k_2, \omega)\right\|\right]^2}{\left\|\mathbf{p}(\mathbf{x}, k_1, k_2, \omega)\right\|^2} \tag{17}$$

  where $\mathbf{p}(\mathbf{x}, k_1, k_2, \omega)$ and $\hat{\mathbf{p}}(\mathbf{x}, k_1, k_2, \omega)$ are the target and reconstructed pressure vectors, respectively and $\|\bullet\|$ represents the Euclidean norm. Note that this relative MSE is a spatial average over the panel. An arbitrary threshold of $-10\,\mathrm{dB}$ (corresponding to a relative MSE of 10%) is chosen in order to gauge the accuracy of the reproduction process. As long as the relative MSE (which will be called the reproduction error in the following) is less than that threshold, the pressure field synthesis will be considered accurate.

Fig. 4 shows the two quantities presented above plotted as functions of frequency and the normalized interplanar distance (with respect to λ_{min}). In Fig. 4a, one can notice that the condition number of the transfer matrix is almost

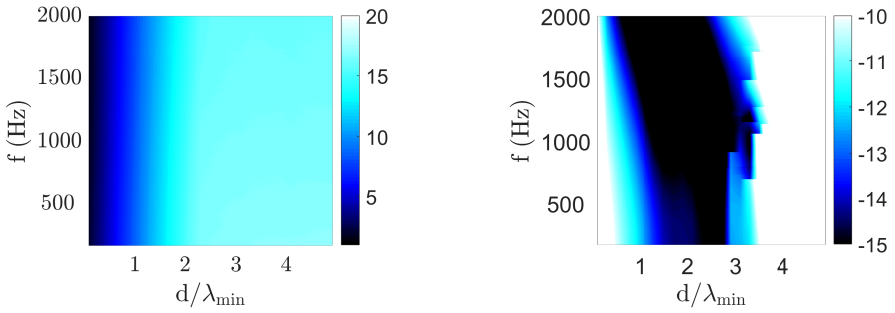

Figure 4: Optimal interplanar distance: (a) logarithm of the condition number ($\log_{10}(\kappa)$) of the transfer matrix, (b) reproduction error e_p (dB, ref. 1) on the reconstructed pressure field according to Eq. (17) for $k_1 = k_{max}$ and $k_2 = 0$. Both quantities are plotted as functions of frequency and the interplanar distance normalized by the smallest wavelength to be synthesized.

frequency independent but increases when the interplanar distance increases. This means that the closer the array of acoustic sources is to the panel plane, the less sensitive the system is to noise. In order to avoid large condition numbers, an upper limit of the interplanar distance d is set to $\frac{\lambda_{min}}{2}$. Concerning the mean square error in Fig. 4b, one observes that it is roughly constant as a function of the frequency for a given interplanar distance. On the contrary, its evolution as a function of the interplanar distance for a given frequency is similar to a U-shaped valley: the error is relatively high when the interplanar distance is small, typically smaller than $\frac{\lambda_{min}}{10}$ or larger than $3\lambda_{min}$. Between these two limits (i.e. for $d \in \left]\frac{\lambda_{min}}{10}, 3\lambda_{min}\right[$), the reproduction error for the maximum wavenumber considered is less than the threshold defined earlier. In the end, the interval in which the interplanar distance d is defined by the intersection of the previous intervals defined from Fig. 4a and Fig. 4b: $I_{opt} = \left]\frac{\lambda_{min}}{10}, \frac{\lambda_{min}}{2}\right[$.

On Fig. 5 the reproduction error e_p is plotted as a function of frequency and wavenumbers in the both directions (i.e. k_1 for Fig. 5a, 5c and k_2 for Fig. 5b, 5d). and for two interplanar distances: one outside the interval I_{opt} and the

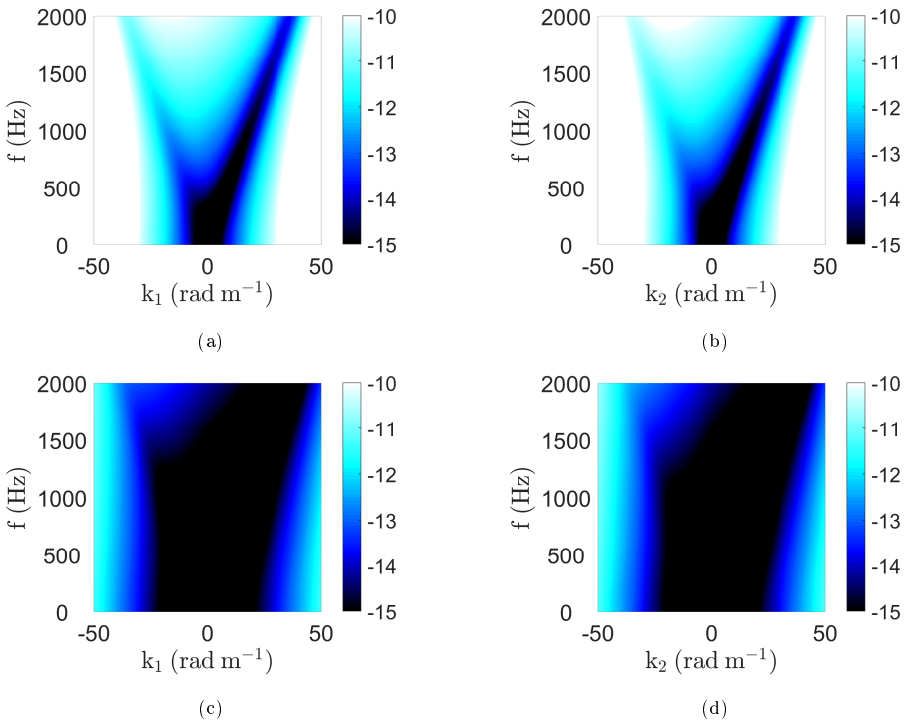

Figure 5: Reproduction error e_p (dB, ref. 1) in the wavenumber-frequency domain for two different interplanar distances. (a) along k_1, $k_2 = 0$ and (b) along k_2, $k_1 = 0$ for $d = \frac{\lambda_{min}}{10}$. (c) along k_1, $k_2 = 0$ and (d) along k_2, $k_1 = 0$ for $d = \frac{\lambda_{min}}{4}$.

other within. There is an almost identical evolution of the reproduction error along k_1 and k_2 directions. One can notice that although the reproduction error in Fig. 5a and 5b complies with the criterion (less than -10 dB) for wavenumbers in the interval $[-30, 30]$ rad m^{-1}, it is not the case for wavenumbers outside this interval. This result was to be expected as the corresponding interplanar distance is not within I_{opt}. On the contrary, in Fig. 5c and 5d one can observe that the reproduction is accurate for all the wavenumbers of interest and that it is in agreement with the proposed criterion as the corresponding interplanar distance is in I_{opt}.

Fig. 6 shows the reproduction error for the same interplanar distance as in

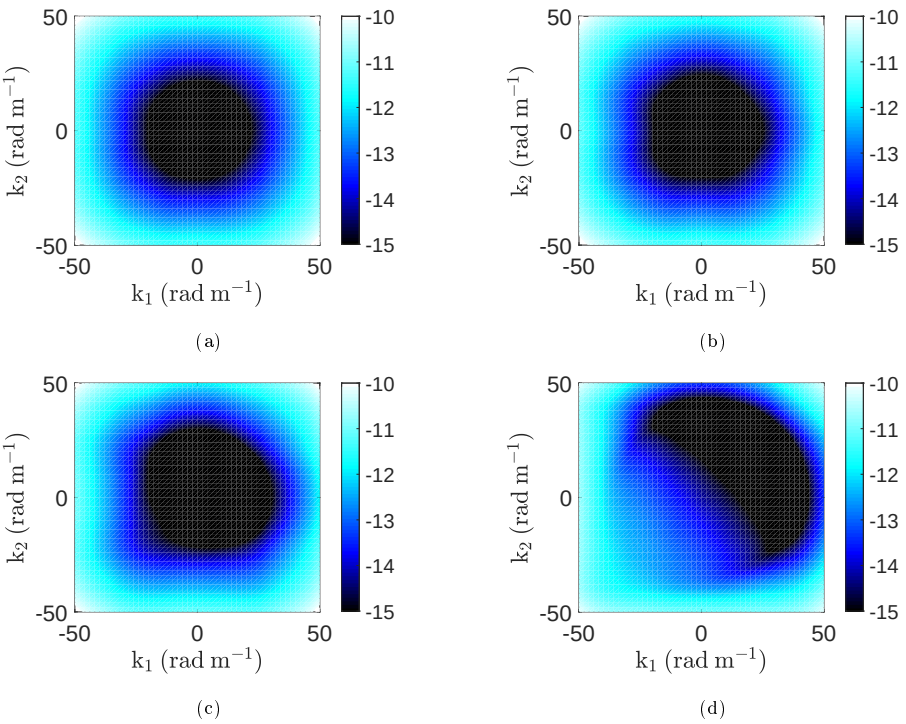

Figure 6: Reproduction error e_p (dB, ref. 1) in the wavenumber domain at (a) $f = 200$ Hz, (b) $f = 500$ Hz, (c) $f = 1000$ Hz and (d) $f = 2000$ Hz for $d = \frac{\lambda_{min}}{4}$.

Fig. 5c and 5d but this time in the wavenumber domain at four different frequencies. One observes that the reproduction error is always below the threshold (see Eq. (17) and discussion). This confirms the consistency of the proposed criterion: for an accurate synthesis, it is preferable to choose the interplanar distance such that $d \in I_{opt}$.

Fig. 7 shows three pressure fields in the spatial domain for a plane wave defined by the wave-vector $(k_1 = 50, k_2 = 50)$ rad m^{-1} at $f = 2000$ Hz which is the most constraining plane wave to reconstruct using the proposed approach as the wavenumbers k_1 and k_2 correspond to the value of the maximum wavenumber used to define the number of source positions. Fig. 7a corresponds to the target pressure field whereas Fig. 7b and 7c correspond to the reconstructed

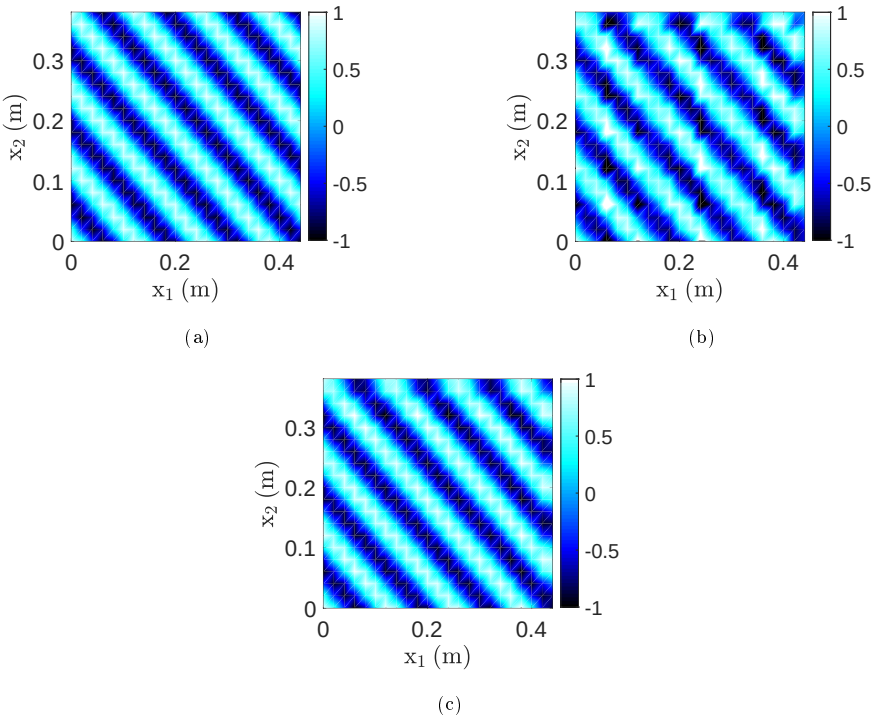

Figure 7: Magnitude of the pressure field (Pa) in the spatial domain at $f = 2000$ Hz for the plane wave defined by $(k_1 = 50, k_2 = 50)$ rad m^{-1}: (a) target, (b) reconstructed for $d = \frac{\lambda_{min}}{10}$ and (c) reconstructed for $d = \frac{\lambda_{min}}{4}$.

pressure field for an interplanar distance outside and inside I_{opt}, respectively. One can notice that although the reproduction error corresponding to the reconstructed pressure field on Fig. 7b does not comply with the set criterion on the entire wavenumber domain (see Fig. 5a and 5b), the proposed method succeeds relatively well to reconstruct the target plane wave. Some errors can be noticed on the amplitude but the shape of the wave is correctly described. On Fig. 7c where the interplanar distance is taken from the interval I_{opt}, the synthesized pressure field is almost identical to the target pressure field. These observations thus validate the chosen interval I_{opt} from which one can choose a value for the interplanar distance.

For the experimental study presented in the following section, the parameters of the array are set to the following values

$$k_{max} = 50\,\mathrm{rad\,m^{-1}},\ \delta_s = 3\,\mathrm{cm} \text{ and } d = 3\,\mathrm{cm}$$

4. Experimental setup

The process of the source scanning technique described in the Sec. 3.1 has been applied on a simply supported aluminum panel. The characteristics of the panel are the same as the one considered in the numerical simulation in Sec. 3.2. To simulate the appropriate boundary conditions (i.e. simply supported), the panel was mounted using the protocol presented by Robin et al. [28] and was placed in a baffle consisting of a 2 cm thick square plywood with a 1 m side and in which there is an aperture the size of the panel, see Fig. 9. The measurements were done in a room where the walls are covered with absorbing wedges and 10 cm thick absorbing foam panels were placed on the floor and around the structure inside the baffle in order to prevent the potential reflections and noises coming from the robot and acquisition system from polluting the measurements.

A mid-high frequency monopole source manufactured by Microflown was used to experimentally simulate the monopole source. This source was placed on the arm of a 3 axis Cartesian robot controlled by a MATLAB script in order to automatize the displacement of the source. It is important to note that this source was only efficient from 300 Hz to 7000 Hz. The considered positions of the source correspond to a regular mesh grid having the size of the panel and located in a plane at $d = 3\,\mathrm{cm}$ of the panel (which is in the interval I_{opt} defined previously). The spacing between two adjacent points is $\delta_s = 3\,\mathrm{cm}$ in the x_1 and x_2 directions. One then has 15 different positions along the x_1 direction and 13 different positions along the x_2 direction, which makes an overall of 195 source positions.

The SST process requires measuring two types of transfer functions:

- In step 2, the transfer functions G_{ps} between source positions s and observation points p: they are measured considering a 2 cm thick square

plywood at the location of the panel as shown in Fig. 8. A linear array of 1/4" ROGA RG-50 microphones flush-mounted at $x_1 = 2\,\text{cm}$ is considered for the measurement of the wall pressure. The microphone spacing is $\delta_p = 2\,\text{cm}$, ensuring a number of observation points P greater than the number of source positions S. Considering a property of invariance in translation of the idealized considered system (i.e. source exciting the baffled panel in a semi-anechoic room), one deduces the pressure distribution on the reconstruction surface for a given source position from measurements with the linear microphone array at different source positions along the x_1 axis with a spacing of $\delta_p = 2\,\text{cm}$. This technical aspect is described in more detail in Appendix B. At the end, we obtained the transfer functions G_{ps} between the $S = 15 \times 13 = 195$ source positions and the $P = 18 \times 20 = 360$ observation points with a frequency resolution of 0.625 Hz. This step is time consuming (i.e. approximately 13 hours for the presented measurement) but it should be achieved only one time to characterize the acoustical environment (i.e. source radiating in the semi-anechoic chamber with the baffle plane). This means that for the characterization of a second structure presenting dimensions smaller or equal to the present one, the same transfer matrix $\mathbf{G}$ could be used.

Figure 8: Measurement of the transfer functions G_{ps}: experimental setup.

Figure 9: Baffled simply supported panel.

- In step 4, $\Gamma_{\alpha}^{s}(\mathbf{x},\omega)$, the FRFs between point $\mathbf{x}$ and the source at position s are determined: they were measured when the test panel was mounted in the baffle as shown in Fig. 9. Two cases depending of the final quantities of interest were considered:

  - to evaluate the panel velocity sensitivity function $H_v(\mathbf{x},\mathbf{k},\omega)$ at a point $\mathbf{x}$ on the panel, the acceleration response at point $\mathbf{x}$ was measured using one Bruel&Kjaer type 4508 accelerometer. The FRFs $\Gamma_{\gamma}^{s}(\mathbf{x},\omega)$ corresponding to the acceleration of the panel at point $\mathbf{x}$ for a monopole source at position s were measured for the $S = 195$ positions. It took approximately 45 minutes to measure all the FRFs $\Gamma_{\gamma}^{s}(\mathbf{x},\omega)$. These latter were used with Eq. (13) to estimate the acceleration sensitivity functions of the panel at point $\mathbf{x}$, $H_{\gamma}(\mathbf{x},\mathbf{k},\omega)$ for $\mathbf{k}$ in $\Omega_{\mathbf{k}}$. Finally , the velocity sensitivity functions were determined using the relation $H_v(\mathbf{x},\mathbf{k},\omega) = \frac{1}{i\omega}H_{\gamma}(\mathbf{x},\mathbf{k},\omega)$ and these quantities were introduced in Eq. (3) with the appropriate model of the wall-pressure fluctuations in order to deduce the power spectral density of the velocity at point $\mathbf{x}$ when the panel is excited by the considered stochastic excitation. It is important to note that the velocity sensitivity functions $H_v(\mathbf{x},\mathbf{k},\omega)$ are determined here using the direct interpretation of Eq. (2) in contrast with the results in

[12] where the reciprocity principle was used by exciting the panel with a shaker at the point of interest $\mathbf{x}$ and measuring the response of the panel on a grid of points using a laser vibrometer. In our case, the grid of monopole source positions constituted the excitation and the response was measured at only one point, the point of interest $\mathbf{x}$, using one accelerometer.

– to evaluate the radiated power by the plate. In accordance with Eq. (6) to (9), the sensitivity functions in term of the radiated pressure and of the particle velocity along x_3-axis should be estimated for the $R = 9 \times 20 = 180$ points discretizing Σ_r. A linear array of microphones close to the panel (at a distance of approximately 7 cm from the panel plane on the radiating side, corresponding to $x_3 = -7$ cm as defined in Sec. 2.2) was used as shown in Fig. 11 to measure the pressure at each point r of Σ_r. To evaluate the particle velocity, an estimation of the pressure gradient was considered.

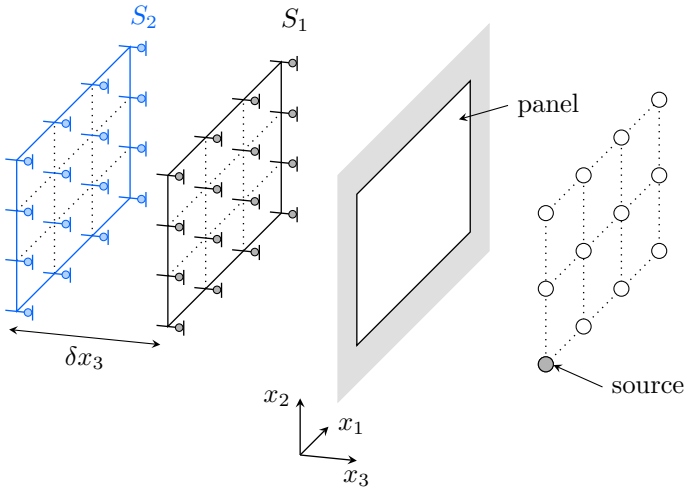

Figure 10: Measurement of the particle velocity with the two microphone method , S_1 and S_2 are discretized surfaces consisting of two identical grids of R points.

With the time dependence $e^{i\omega t}$, the particle velocity at direction x_3 can be

written

$$v_0^{x_3} = -\frac{i}{\rho_0 \omega} \frac{\partial p}{\partial x_3} \tag{18}$$

Thus, the particle velocity can be obtained by evaluating the pressure gradient $\partial p / \partial x_3$ [29, 30] by using the two point finite difference method

$$v_0^{x_3} \approx -\frac{i}{\rho_0 \omega} \frac{p_2 - p_1}{\delta x_3} \tag{19}$$

where p_1 and p_2 are pressure measurements at two adjacent positions on surface S_1 and on surface S_2, respectively, as shown in Fig. 10. δx_3 is the spacing between the two surfaces S_1 and S_2 and is also the distance between two microphone positions on the grid. δx_3 must be large enough to induce a sufficient pressure difference in order to determine the particle velocity but it also must be small enough for the approximation in Eq. (19) to be valid. Some trial and error tests with the monopole were made in order to define an adequate spacing between the two planes where the pressure would be measured and it was found out that a separation of $\delta x_3 \approx 2\,\text{cm}$ was ideal for these measurements. Normally, the finite difference method suffers from robustness issue against sensor noise and mismatch but the latter is avoided here as the particle velocity at one position of the grid in Fig. 10 is obtained using two pressure measurements of the same microphone at the designated position (see Fig. 10 for an illustration of the proposed methodology). In the experimental setup, only one linear array of 20 microphones is used to accomplish these pressure measurements on the two surfaces S_1 and S_2. In fact the linear array of microphone is mounted on a $2D$ Cartesian robot allowing us to sweep through a given surface on the radiating side of the panel. Measuring the transfer functions $\Gamma_p^s(\mathbf{x}, \omega)$ (radiated pressure) and $\Gamma_{v_0}^s(\mathbf{x}, \omega)$ (particle velocity) at point $\mathbf{x}$, now located on the discretized surface Σ_r, allows us to determine the pressure sensitivity functions $H_p(\mathbf{x}, \mathbf{k}, \omega)$ and the particle velocity sensitivity functions $H_{v_0}(\mathbf{x}, \mathbf{k}, \omega)$ used in Eq. (8). The measurement of all the transfer functions needed in the determination of the radiated power by the panel took approximately 46 hours.

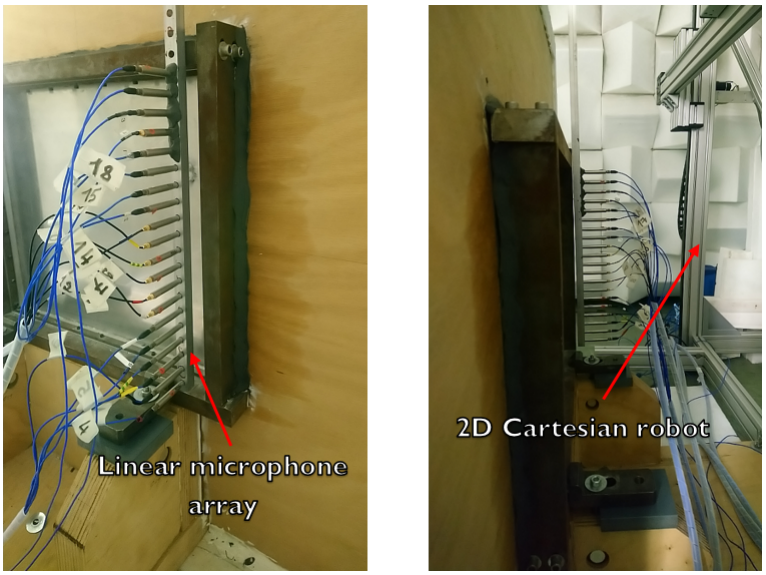

Figure 11: Particle velocity measurements: experimental setup.

5. Results and discussion

5.1. Numerical validation

In order to assess the accuracy of the SST process on the test panel, one proposes in this section to compare its results with numerical ones. As evoked in Sec. 3.2, these latter were achieved using the analytical normal modes and the modal expansion method as described in Appendix B. First, let us compare the velocity sensitivity functions experimentally estimated with the SST process with the ones estimated numerically at point $\mathbf{x} = (0.06, 0.3, 0)$ m. The results are plotted in Fig. 12 as a function of the frequency and the wavenumber, k_1 for $k_2 = 0$. A good agreement between both results can be observed, even for wavenumbers above the acoustic wavenumbers (which are symbolized by the continuous white line in Fig. 12). This highlights that the SST approach is well adapted for reproducing subsonic plane waves, which is a limitation of past-developed reproduction techniques [4, 8, 10]. Below 300 Hz, one can however observe that the SST results are noisy. For these frequencies, the monopole source was not efficient and the measurements of the transfer functions were

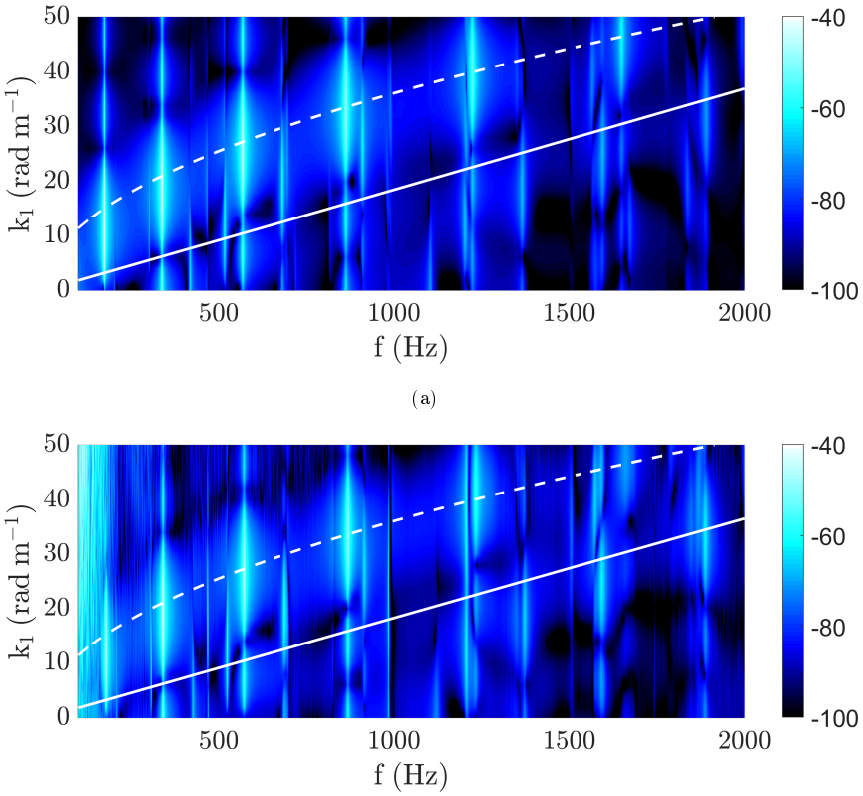

Figure 12: Velocity sensitivity functions $|H_v(\mathbf{x}, k_1, k_2 = 0, \omega)|^2$ (dB, ref. $1\,\mathrm{m^3\,s^{-1}\,Pa^{-1}}$): (a) numerical and (b) SST. Continuous white line: acoustic wavenumber k_0. Dashed white line: panel flexural wavenumber k_f.

polluted by the background noise. On the other hand, in the higher part of the frequency range, some discrepancies between the two approaches appear. They can be attributed to the difference between the model that supposed a panel, perfectly simply supported on its four edges and the experimental one that approaches these conditions with thin blades.

Fig. 13 and 14 show the ASD function of the structural velocity response at the receiving point $\mathbf{x} = (0.06, 0.3, 0)$ m (in dB units) when excited by a DAF and a TBL pressure field, respectively, as described in Sec. 2.1.1 and 2.1.2.

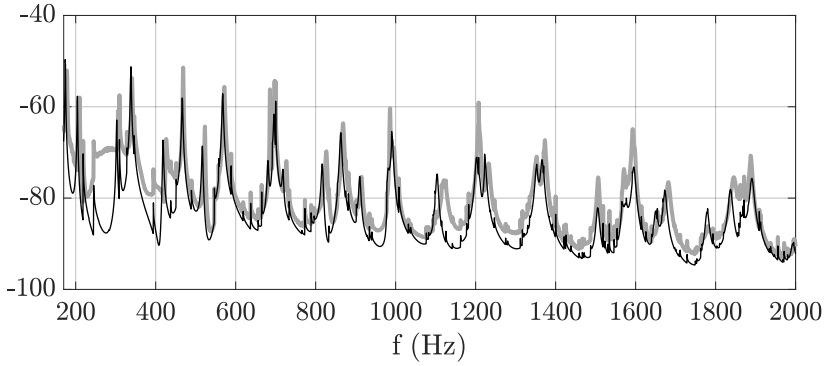

Figure 13: Velocity ASD function $S_{vv}(\mathbf{x}, \omega)$ (dB, ref. $1\,\mathrm{m^2\,s^{-2}\,Hz^{-1}}$) of the panel subjected to a DAF excitation: numerical (thin black line), SST (thick gray line).

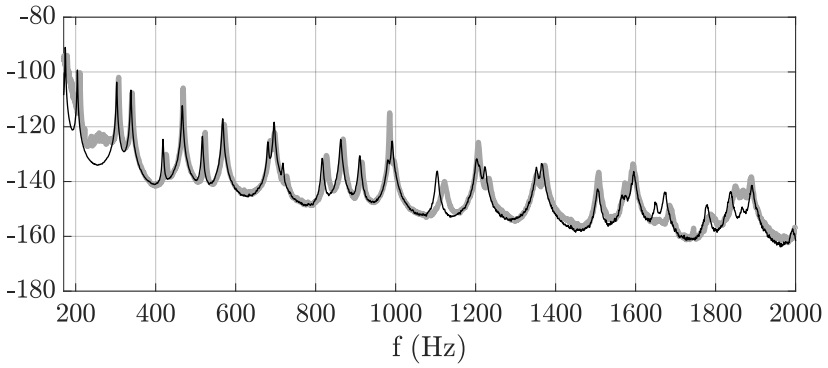

Figure 14: Velocity ASD function $S_{vv}(\mathbf{x}, \omega)$ (dB, ref. $1\,\mathrm{m^2\,s^{-2}\,Hz^{-1}}$) of the panel subjected to a TBL excitation: numerical (thin black line), SST (thick gray line).

It can be observed that the vibration responses, in both the DAF and TBL excitation cases, determined using SST do not match the numerical ones between approximately 230 Hz and 300 Hz: this is due to the fact that the source is not efficient in that frequency range as stated before. The vertical offsets that can be observed at some frequencies are due to the fact that for the numerical case, the modal damping of the panel is taken constant over the entire frequency range (i.e. $\eta = 0.005$) whereas it is certainly dependent on the panel modes

in real conditions (see the values measured by Marchetto for the first modes in Table II, Ref. [12]). It can also be noticed that the vibration response in the DAF case is higher than in the case of the TBL excitation: this is due to the fact that the modes that contribute to the panel response under a diffuse field excitation are more efficiently excited than in the case of a TBL excitation [16].

Now, let us focus on the panel radiation. Fig. 15 and 16 show the inverse of the radiated power (in dB units) by the panel when excited by a DAF and a TBL pressure field, as described in Sec. 2.1.1 and 2.1.2 respectively.

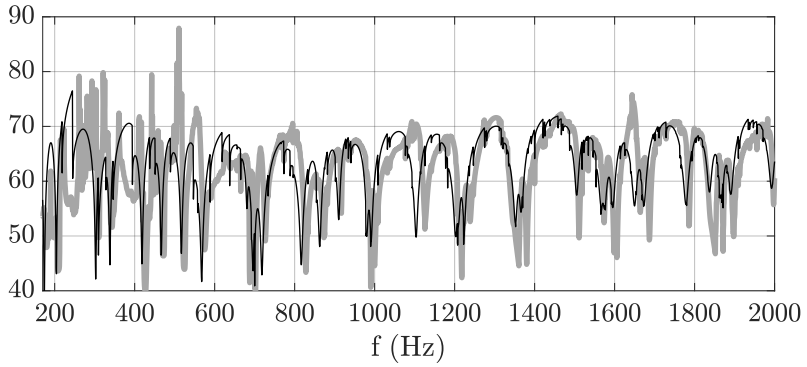

Figure 15: Inverse of the radiated power $\Pi_r(\omega)$ (dB, ref. $1\,\mathrm{W^{-1}\,Hz}$) by the panel under DAF: numerical (thin black line), SST (thick gray line).

The radiated power was determined using the two microphones method for the SST approach. For both cases (DAF and TBL), the experimental results do not match the theoretical results under approximately 700 Hz: this is probably due to the fact that the monopole source was not very efficient to induce a sufficient radiation amplitude for the measurement of the pressure and particle velocity sensitivity functions. Moreover, the estimation of the particle velocity with the two microphone measurements can amplify the uncertainties. From a practical point of view, one can conclude that an acoustic source more efficient in the low frequency range would be required. In general, this type of source (such as loudspeakers) has a greater size than the considered one, that would require to define a coarser mesh for the source positions. With the present

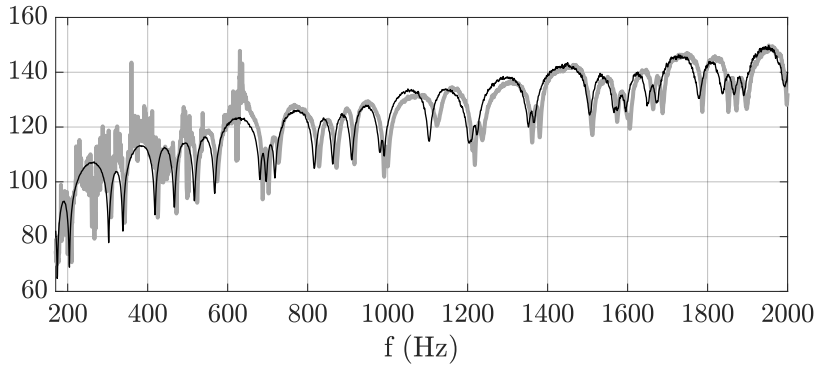

Figure 16: Inverse of the radiated power $\Pi_r(\omega)$ (dB, ref. $1\,\mathrm{W}^{-1}\,\mathrm{Hz}$) by the panel under TBL: numerical (thin black line), SST (thick gray line).

source, one can however observe a good agreement between the SST results and the numerical ones for both excitations. The two curves match very well above 700 Hz for the TBL excitation. That shows that the subsonic plane waves are well synthesized by the SST (as it has been already observed in Fig. 12).

In conclusion of this section, there is globally a good agreement between the numerical results and those obtained from the proposed method as well as in terms of the panel vibrations and the radiated sound power. For this latter quantity, the strength of the acoustic source did not permit however a satisfactory reproduction below 700 Hz.

5.2. Experimental validation with measurements in standard test facilities

In this section, the experimental results obtained with the proposed SST method are compared to results obtained in standard test facilities. The results obtained in the standard test facilities have already been published [11, 12] and were done at the University of Sherbrooke by Marchetto et al. They concern the vibrations of a similar panel. In Ref. [11], the panel is excited by a DAF experimentally generated within a reverberant room whereas as in Ref. [12], it is excited by a turbulent flow generated in an anechoic wind tunnel at a flow speed of $20\,\mathrm{m\,s}^{-1}$. More details on these measurements can be found in these

references.

Fig. 17 and 18 show for the DAF and the TBL, respectively, a comparison of the panel vibration responses obtained with the SST and the standard test facilities.

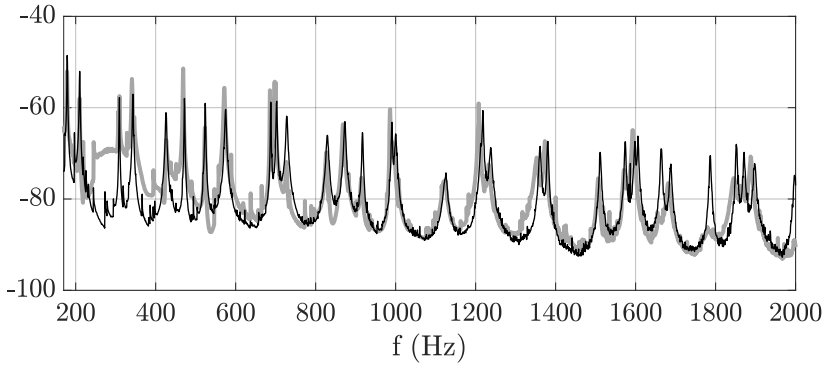

Figure 17: Velocity ASD function $S_{vv}(\mathbf{x}, \omega)$ (dB, ref. $1\,\mathrm{m^2\,s^{-2}\,Hz^{-1}}$) of the panel subjected to a DAF excitation: reverberant chamber measurements at the University of Sherbrooke [11] (thin black line), SST (thick gray line).

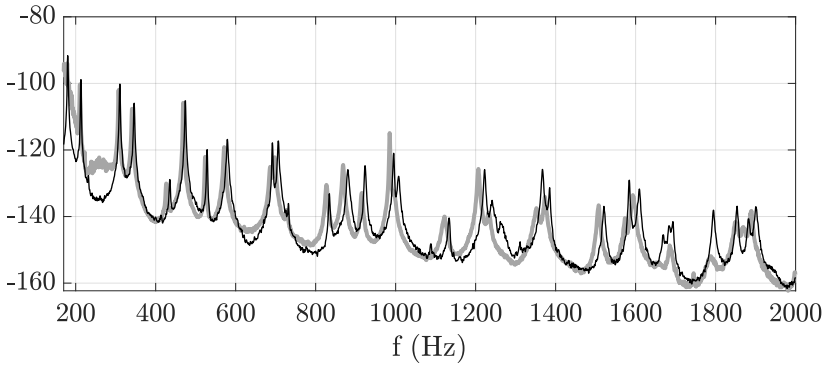

Figure 18: Velocity ASD function $S_{vv}(\mathbf{x}, \omega)$ (dB, ref. $1\,\mathrm{m^2\,s^{-2}\,Hz^{-1}}$) of the panel subjected to a TBL excitation: wind tunnel measurements at the University of Sherbrooke [12] (thin black line), SST (thick gray line).

There is globally a good agreement between the results obtained using SST

and those measured in the test facilities. One can notice a shift of the responses along the frequency axis which is due to the fact that the panel used in the test facilities is not exactly the same as the one used in our experiment although both panels are made out of aluminum and have the same dimensions. This shift can also be explained by some minor differences in the boundary conditions. These results show well that the proposed SST is able to reproduce the excitation of a standard test facility.

6. Conclusion

This paper presented an experimental process for the characterization of structures under random excitations by using a single acoustic source combined with the synthetic array principle: the monopole source is displaced to different positions allowing to mimic the effect of a full array and to reproduce the target wall-pressure field, hence the name of *source scanning technique*. This process can be seen as alternative or complementary to standard test facilities such as reverberant rooms or wind tunnels. A previous paper had already established the principle of this approach and gave promising preliminary results. In the present study, our attention was focused on the validation of the process with comparisons against numerical and experimental results obtained with test facilities such as the reverberant room and the anechoic wind tunnel. A parametric study based on numerical simulations aiming at defining the ideal design of the array of virtual sources was done. This study allowed to define an optimal interval I_{opt}, for the distance between the panel and the source array, in which the pressure field synthesis is in good agreement with the target pressure field, allowing a good reproduction of the vibroacoustic response of the considered structure.

The proposed method was applied on a simply supported aluminum panel which was subject to either DAF or TBL excitation. Both the velocity response at a given point and the radiated power by the panel were estimated. A $3D$ Cartesian robot was used to move the acoustic source whereas a $2D$ Carte-

sian robot was used to move a linear array of microphones. This system was controlled by a MATLAB script that allows us to automatize the measurement process of the transfer functions between the source at different positions and the quantities of interest. To evaluate the radiated power, the two microphone method was used to estimate the normal particle velocity. Apart from an overestimation of the panel responses between 230 and 300 Hz due to the low efficiency of the monopole source and the noisy radiated power under approximately 600 Hz stemming from the two microphone method, there is a fairly good agreement between the three types of results (numerical, SST and direct measurements).

The total measurement time of the transfer functions needed to determine the velocity response as well as the radiated power by the panel is approximately 60 hours. The measurement of the transfer functions needed to determine the radiated power by the panel are the most time consuming (approximately 46 hours) as it required to measure the radiated pressure and to estimate the acoustic velocity using a linear array of microphone. The use of acoustic velocity probes as well as a larger microphone array could greatly reduce these measurement times. These ones are however not completely penalizing as the process is fully automatized. Moreover, compared to standard facilities, the process supplies the sensitivity functions that can give some insights on how the structure filters out the random excitation.

As the SST process has been validated and automatized, it can be used in the future to compare the responses of different complex panels under DAF or TBL excitation. As the considered excitation will be represented by a model, the comparison between different panels will not be perturbed by uncertainties and background noises related to the excitation. Moreover, the analysis of the measured sensitivity functions will be helpful to extract the physical phenomena contributing to the noise radiation of the panels.

Acknowledgments

This work was funded by the French National Research Agency (VIRTECH project, ANR-17-CE10-0012) and was performed within the framework of the LABEX CeLyA (ANR-10-LABX-0060) of Université de Lyon, within the program « Investissements d'Avenir » (ANR-16-IDEX-0005) operated by the French National Research Agency (ANR).

Appendix A. Numerical calculation of the sensitivity functions

The sensitivity functions characterize the dynamical behavior of a given structure and have been defined by Eq. (2). For the considered panel in this study, these sensitivity functions are calculated using the modal expansion method

$$H_v\left(\mathbf{x},\mathbf{k},\omega\right)=i\omega\sum_{m,n}\frac{F_{mn}\left(\mathbf{k}\right)\phi_{mn}\left(\mathbf{x}\right)}{M_{mn}\left(\omega_{mn}^2-\omega^2+i\eta_{mn}\omega_{mn}\omega\right)} \tag{A.1}$$

where m and n are both positive integers related to the summations.

- $\mathbf{x}=(x_1,x_2,0)$ is the point of interest on the panel surface,
- $F_{mn}\left(\mathbf{k}\right)$ is called the generalized force of the plane wave,
- $\phi_{mn}\left(\mathbf{x}\right)$ represents the mode shape, M_{mn} the modal mass, ω_{mn} the modal angular frequency and η_{mn} the modal damping.

For a simply supported panel on all edges (as shown in Fig. 1), the modal parameters are given in the following equations

$$\omega_{mn}=\left[\left(\frac{m\pi}{L_1}\right)^2+\left(\frac{n\pi}{L_2}\right)^2\right]\sqrt{\frac{D}{\rho h}} \tag{A.2}$$

$$\phi_{mn}(\mathbf{x})=\sin\left(\frac{m\pi}{L_1}x_1\right)\sin\left(\frac{n\pi}{L_2}x_2\right) \tag{A.3}$$

$$M_{mn}=\frac{\rho h L_1 L_2}{4} \tag{A.4}$$

The modal force is given by

$$F_{mn}\left(\mathbf{k}\right)=\int\int_{\Sigma_p}p\left(\mathbf{x},\mathbf{k}\right)\phi_{mn}\left(\mathbf{x}\right)\mathrm{d}\mathbf{x} \tag{A.5}$$

where Σ_p designates the area of the panel and $p\left(\mathbf{x},\mathbf{k}\right)=e^{-i\mathbf{kx}}$ is the prescribed pressure field corresponding to a unit wall plane wave characterized by the wave-vector $\mathbf{k}$.

Equation (A.5) has a closed-form solution

$$F_{mn}\left(\mathbf{k}\right)=F_{mn}\left(k_1,k_2\right)=I_m^1\left(k_1\right)I_n^2\left(k_2\right) \tag{A.6}$$

where for $\xi \in \{1,2\}$ and $p \in \{m,n\}$

$$I_p^{\xi}(k_\xi) = \begin{cases} \left(\dfrac{p\pi}{L_\xi}\right) \dfrac{(-1)^p e^{-jk_\xi L_\xi} - 1}{k_\xi^2 - \left(\frac{p\pi}{L_\xi}\right)^2} & \text{if} \quad |k_\xi| \neq \dfrac{p\pi}{L_\xi} \\ \dfrac{1}{2} j L_\xi \quad \text{otherwise} \end{cases} \tag{A.7}$$

Appendix B. Source characterization strategy using a single linear array of microphones: Invariance Principle

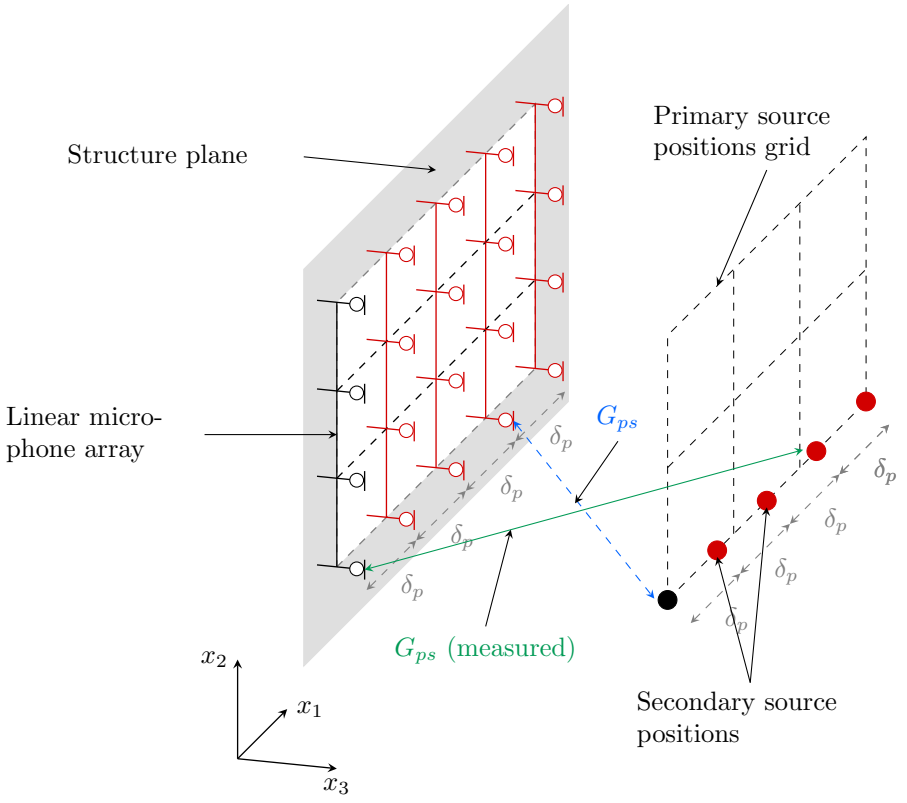

Figure B.19: FRFs measurements using a non-displaceable microphone array

The second step of the SST process requires the measurement of the FRFs G_{ps} between the source position s and the observation p on the reconstruction surface. A linear flush-mounted microphone array was used to achieve this measurement. As this array does not cover the whole reconstruction surface, one used the invariant property in translation of the idealized considered system (i.e. source, flat baffle, semi-anechoic room) to deduce the required transfer functions. This is highlighted in Fig. B.19.

The blue grid shows the primary positions occupied by the source if we had

a rectangular array or a displaceable (with an actuator for instance) linear array of microphones. The secondary source positions in red are the additional source positions needed to measure the FRFs if one had a single non-displaceable linear array of microphones considering the invariance property in translations. Thus, instead of measuring, for instance, the blue (dashed) FRF (see Fig. B.19), one would displace the source at the position facing the linear microphone array (same x_1 coordinate but different x_3 coordinate) and measure the green (solid line) FRF G_{ps}. As the linear array is along the x_2 axis, there is no need to displace the source along the x_2 coordinate. With this methodology, one can measure the transfer function G_{ps} for any point on the reconstruction surface with the considered linear array.

References

[1] F. J. Fahy, On simulating the transmission through structures of noise from turbulent boundary layer pressure fluctuations, Journal of Sound and Vibration 3 (1) (1966) 57–81.

[2] C. Maury, S. J. Elliott, P. Gardonio, Turbulent Boundary-Layer Simulation with an Array of Loudspeakers, AIAA Journal (2004) 706–713.

[3] S. J. Elliott, C. Maury, P. Gardonio, The synthesis of spatially correlated random pressure fields, The Journal of the Acoustical Society of America (2005) 1186–1201.

[4] T. Bravo, C. Maury, The experimental synthesis of random pressure fields: Methodology, The Journal of the Acoustical Society of America (2006) 2702–2711.

[5] C. Maury, T. Bravo, The experimental synthesis of random pressure fields: Practical feasibility, The Journal of the Acoustical Society of America (2006) 2712–2723.

[6] M. Aucejo, L. Maxit, J. L. Guyader, Experimental simulation of turbulent boundary layer induced vibrations by using a synthetic array, Journal of Sound and Vibration 331 (16) (2012) 3824–3843.

[7] C. Maury, T. Bravo, Focussed Synthesis of a Turbulent Boundary Layer Excitation, 22nd AIAA/CEAS Aeroacoustics Conference (May 2016).

[8] A. Berry, R. Dia, O. Robin, A wave field synthesis approach to reproduction of spatially correlated sound fields, The Journal of the Acoustical Society of America 131 (2) (2012) 1226–1239.

[9] O. Robin, A. Berry, S. Moreau, Reproduction of random pressure fields based on planar nearfield acoustic holography, The Journal of the Acoustical Society of America 133 (6) (2013) 3885–3899.

[10] O. Robin, A. Berry, S. Moreau, Experimental vibroacoustic testing of plane panels using synthesized random pressure fields, The Journal of the Acoustical Society of America 135 (6) (2014) 3434–3445.

[11] C. Marchetto, L. Maxit, O. Robin, A. Berry, Vibroacoustic response of panels under diffuse acoustic field excitation from sensitivity functions and reciprocity principles, The Journal of the Acoustical Society of America 141 (6) (2017) 4508–4521.

[12] C. Marchetto, L. Maxit, O. Robin, A. Berry, Experimental prediction of the vibration response of panels under a turbulent boundary layer excitation from sensitivity functions, The Journal of the Acoustical Society of America 143 (5) (2018) 2954–2964.

[13] F. J. Fahy, Some applications of the reciprocity principle in experimental vibroacoustics, Acoustical Physics 49 (2) (2003) 217–229.

[14] S. W. Autrey, Passive synthetic arrays, The Journal of the Acoustical Society of America 84 (2) (1988) 592–598, publisher: Acoustical Society of America.

[15] F. J. Fahy, P. Gardonio, Sound and Structural Vibration: Radiation, Transmission and Response, 2nd Edition, Academic Press, Amsterdam ; Boston, 2006.

[16] C. Maury, P. Gardonio, S. J. Elliott, A Wavenumber Approach to Modelling the Response of a Randomly Excited Panel, Part I: General Theory, Journal of Sound and Vibration 252 (1) (2002) 83–113.

[17] L. Maxit, V. Denis, Prediction of flow induced sound and vibration of periodically stiffened plates, The Journal of the Acoustical Society of America 133 (1) (2013) 146–160.

[18] I. 10140-2:2010, Acoustics – Laboratory measurement of sound insulation of building elements – Part 2: Measurement of airborne sound insula-

tion, Standard, International Organization for Standardization, Geneva, CH (2010).

[19] A. E90-09, Standard Test Method for Laboratory Measurement of Airborne Sound Transmission Loss of Building Partitions and Elements, Standard, ASTM International, West Conshohocken, PA (2009).

[20] I. 15186-1:2000, Acoustics – Measurement of sound insulation in buildings and of building elements using sound intensity – Part 1: Laboratory measurements, Standard, International Organization for Standardization, Geneva, CH (2000).

[21] A. E2249-02, Standard Test Method for Laboratory Measurement of Airborne Sound Transmission Loss of Building Partitions and Elements Using Sound Intensity, Standard, ASTM International, West Conshohocken, PA (2016).

[22] R. K. Cook, Measurement of Correlation Coefficients in Reverberant Sound Fields, Acoustical Society of America Journal 27 (6) (1955) 1072.

[23] W. K. Blake, Mechanics of Flow-Induced Sound and Vibration, Volume 2: Complex Flow-Structure Interactions, Academic Press, 2017.

[24] R. H. Mellen, On modeling convective turbulence, The Journal of the Acoustical Society of America 88 (6) (1990) 2891–2893.

[25] F. Fahy, Sound intensity, Elsevier Applied Science, 1989.

[26] J. C. Curlander, R. N. McDonough, Synthetic Aperture Radar: Systems and Signal Processing, 1st Edition, Wiley-Interscience, New York, 1991.

[27] E. Cheney, D. Kincaid, Numerical Mathematics and Computing, Cengage Learning, 2007.

[28] O. Robin, J.-D. Chazot, R. Boulandet, M. Michau, A. Berry, N. Atalla, A Plane and Thin Panel with Representative Simply Supported Boundary

Conditions for Laboratory Vibroacoustic Tests, Acta Acustica united with Acustica 102 (1) (2016) 170–182.

[29] M. R. Bai, S.-W. Juan, C.-C. Chen, Particle velocity estimation based on a two-microphone array and Kalman filter, The Journal of the Acoustical Society of America 133 (3) (2013) 1425–1432, publisher: Acoustical Society of America.

[30] A. D. Pierce, Acoustics: An Introduction to Its Physical Principles and Applications, Acoustical Society of America, 1989.